Efficient Insertion of Partially Flexible Objects in Precision Assembly

Dengpeng Xing, Fangfang Liu, Song Liu, and De Xu, *Senior Member, IEEE*

***Abstract*— This paper proposes an efficient strategy for the insertion of the partially flexible object in precision assembly. The partially flexible object refers to the component with unevenly distributed flexibilities: coupling rigidity and flexibility. This paper focuses on the insertion of one class of partially flexible objects: rigid shapes connected by a compliant mechanism. We first analyze the horizontal compliance of the compliant mechanism and build a model to relate its state and force. The insertion is separated into two stages according to the insertion type. The first stage is a compliant insertion and we estimate the insertion direction based on the built model, horizontally compensate resorting to the horizontal compliance and the updated direction, and efficiently plan the vertical insertion in an aggressive strategy regarding the uncertainties caused by the compliant mechanism and predicting the future insertion. The second stage is a hybrid insertion with both rigid and compliant gripping and its features include that the object states are not precisely measurable and the motion of a part of the object is not directly controllable. To solve it, we qualitatively and quantitatively analyze all possible configurations and, taking advantage of the insertion property, conclude one insertion posture based on which a control strategy is proposed. Additionally, a conservative insertion strategy is planned resorting to the past execution performance and the current state evaluation. Experiments are carried out to demonstrate the validation of the proposed method.**

***Note to Practitioners*—This paper was motivated by the problem of inserting partially flexible objects in precision assembly, but it also applies to other components with unevenly distributed flexibilities. This approach has benefits in terms of assembling rigid-compliant-rigid sets of the objects and modeling the behavior of many similar objects. The following key steps are mentioned to apply the proposed method. The practitioners need to first compute the insertion compliance based on the model that is built in this paper to relate the deformation and force. The determination of the object configuration in hybrid insertion is then demanded considering the system compliance. The final steps are to obtain the object states according to the force output and efficiently plan the insertion depths considering the past performance, the current evaluation, and the future prediction. In future research, we will address the simultaneous assembly of multiple partially flexible objects.**

***Index Terms*— Efficient insertion, partially flexible object, precision assembly.**

Manuscript received April 3, 2018; revised May 23, 2018; accepted July 2, 2018. Date of publication July 24, 2018; date of current version April 5, 2019. This paper was recommended for publication by Associate Editor S. Jeon and Editor K. Saitou upon evaluation of the reviewers' comments. This work was supported in part by the Science Challenge Project under Grant TZ2018006-0204-02 and in part by the National Nature Science Foundation of China under Grant 61673382, Grant 61741317, and Grant 61733004. *(Corresponding author: Dengpeng Xing.)*

D. Xing, F. Liu, and D. Xu are with the Institute of Automation, Chinese Academy of Sciences, Beijing 100190, China, and also with the University of Chinese Academy of Sciences, Beijing 101407, China (e-mail: dengpeng.xing@ia.ac.cn).

S. Liu is with the City University of Hong Kong, Hong Kong.

Color versions of one or more of the figures in this paper are available online at http://ieeexplore.ieee.org.

Digital Object Identifier 10.1109/TASE.2018.2853607

I. Introduction

DIFFERENT from traditional assembly, precision assembly deals with small objects, with sizes ranging from micrometers to millimeters, and tolerances within the same size range. It consists of two phases: alignment and insertion [1]. In alignment, precision assembly uses two or more microscopes to provide accurate visual feedback and precise actuators to place objects where they are approximately aligned [2]. The insertion phase employs an accurate force sensor to detect the contact between objects, compensates for their misalignment, and inserts them into the desired location [3]. Wide attention has been received in precision assembly [4] and many accomplishments have been attained so far.

In the domain of precision assembly, different topics are discussed to facilitate accurate insertion. For assembly plan, a general strategy [5] is proposed to investigate precision assembly combining several subprocesses on a platform with multiple robot arms, and assemblies in interference fit and clearance fit are individually treated. For assembly in multiscale, Das *et al.* [6] arrange several reconfigurable modules for a system with multiple custom-designed end-effectors depending on the specific task. For capability enhancement of dealing with disturbances, an inclined insertion strategy is presented in [7] to compensate for the deviated insertion direction by coordinating manipulators. For efficiency improvement, an insertion strategy is presented in [8] for the precision assembly of cylindrical components with an interference fit, by modeling the insertion as a stochastic state transition process with the uncertainty described by Gaussian distribution and choosing an action after iterative calculations in an estimation manner. Most of the insertion studies in precision assembly focus on the acquirement of high precision and the way to react with the contact feedback, and the objects are usually held firmly by rigid grippers [9]. However, those methods require a good alignment before insertion and calibration of robotic arms, and the insertion fails if disturbance is large.

Different from rigid or fully flexible components, a partially flexible object has unevenly distributed compliance, coupling the rigidity and flexibility together [10]. It has various applications, e.g., flip chip assembly of rigid and flexible polymer substrates, the flex-rigid printed circuit board [11], rigid-link

flexible-joint robot [12], and so on. Assembling these flexible and rigid parts is a topic that has been investigated recently. The flexible sensors for minimally invasive instruments are assembled on a flex-to-rigid platform [13], where flexible interconnections are laid between the different parts of the sensor system. In [14], a compliant safe joint is assembled to passively achieve multiple working states behaving as a rigid or flexible joint according to the load. To consider the part deformation in rigid assemblies, rigid and compliant variation models are developed to better evaluate the dimensional quality of sheet metal assembly [15]. Due to the property of partially flexible objects, their insertion involves hybrid clamping including the rigid and compliant clamping, which is still a challenge for precision assembly.

The way the object is gripped determines the insertion type. Rigid clamping, the most commonly used in precision assembly, firmly holds objects, and active compliant methods, such as hybrid position/force control [16] and impedance control [17], are employed to increase the system compliance. These strategies are based on the measured force and no large misalignment is allowed. Compliant clamping, on the contrary, grips objects with compliant mechanisms, and in the corresponding compliant DOFs, the object is automatically adjusted according to the contact, providing passive compliance [18], [19]. A robust impedance control for position and force regulation of a compliant gripper is presented in [20], enabling a smooth transition between free and constrained motions of the gripper. In [21], a microremote center compliance unit and a microgripper are used to support the assembly system with low translational and rotational stiffness. This clamping accepts more misalignments but has the difficulty of generalized application. Those works focus on either of compliance and seldom mention to combine them together, using both the compliance types to fulfill a multiple process insertion.

Our motivation is to develop an efficient insertion strategy dedicated for partially flexible objects with an interference fit in precision assembly. Specifically, we deal with the difficulties in efficient hybrid insertion where the rigid and compliant clamping types are coupled, the insertion is uncertain caused by the compliant mechanism, and the object state is immeasurable. This paper first builds a model to relate the state of the compliant mechanism with the force on it and analyzes the horizontal stiffness of the compliant configuration. In the compliant assembly, we present a control strategy in the presence of uncertainty, in which the insertion direction is online-estimated and an aggressive insertion is planned after evaluating the past experience, the current states, and the future prediction. A hybrid insertion combining rigid and compliant clamping is then studied and an insertion strategy is proposed where the accurate state is immeasurable and the compliant part is uncontrollable. An efficient insertion is conservatively regulated based on an iterated parameter reflecting the past effect and the current evaluation. For possible application, the proposed method facilitates not only assembling partial flexible objects in the domain of precision assembly, but also benefiting the behavior modeling of many objects with rigid-compliant-rigid sets.

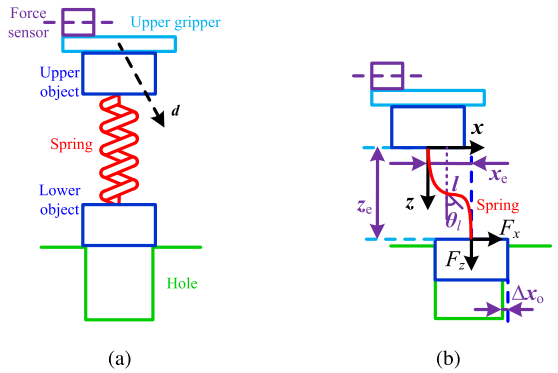

Fig. 1. Configuration and force analysis in insertion. (a) Initial configuration. (b) Spring in compression.

The contributions of this paper include the following.

1) In precision assembly, we investigate on the insertion of a partially flexible object with an interference fit. It includes a compliant insertion and a hybrid one with both rigid and compliant properties.
2) Control strategies are proposed for different insertion types, where the insertion direction is online-estimated based on the built compliant model and the problem of immeasurable accurate states is solved after analyzing all possible configurations and presenting an assumption given the insertion property.
3) In the presence of the uncertainty, an aggressive strategy is planned for the compliant insertion by predicting the future insertion ratio according to the past performance and evaluating the current horizontal contact and the estimation of the insertion direction. Meanwhile, the hybrid insertion uses a conservative strategy based on an iterated parameter reflecting the past performance and the current state evaluation.

II. Compliance Discussion

A. Configuration

We use an object combining two rigid cylinders connected by a spring as a prototype to study the insertion of a partially flexible object. The compliant mechanism can be other type and the reason that a spring is chosen is due to its flexibility of compression, transverse, and bending. The strategy proposed in this paper can also be applied to other similar partially flexible objects. The insertion configuration is shown in Fig. 1(a): a force sensor is laid upon the upper gripper, which holds the partially flexible object and the hole is held still by a lower gripper. The spring's ends are fixed on both the cylinders, and in its natural state the spring is aligned with the cylinders. The insertion is vertical, with $\boldsymbol{d}$ as the approaching direction of the cylinder-spring set, and the angular deviation of the axes between the cylinders and the hole is equal to zero, which can be achieved in the alignment process. The target is to insert the partially flexible object totally into the hole with an interference fit between them. The hole's length is a little shorter than the sum of two cylinders' lengths and the spring's free length, which means after insertion, the spring stores energy and stress forces exist upon the cylinders. During insertion, the spring is in compression, and if there is a

horizontal force on the spring's end, the cylinders are deviated from the hole's center in different sides, as shown in Fig. 1(b) where the compressed spring pushes the lower cylinder on the other side of the hole. As stated above, the insertion direction of the upper gripper is along $\boldsymbol{d}$.

The interference in insertion results in the always-existing force that is exerted on the object by the hole, and the effects of this force include the following.

1) The increment in insertion difficulty, since in precision assembly, the small-sized and thin-walled objects are easily broken.
2) The axial force between the lower cylinder and the hole equals the spring vertical force, which compresses the spring. This force leads to the insertion depth inequality of the two cylinders, bringing uncertainties in insertion planning.
3) Although the accurate states of both the cylinders are unknown when they are inserted into the hole, the configuration can still be obtained due to the constraints from the interference insertion.

B. Spring State Computation

As stated above, the spring is firmly connected with the cylinders at its two ends, rather than connected by a spherical bearing, and suffering from a horizontal force at its end, the spring will be curve shaped instead of keeping straight. This leads to a difficulty in correlating the spring force with the offset between the spring's two ends. Suppose the spring is homogeneous, which means, in the case of bending, the bending degree of every part of the spring is the same. In precision assembly, accurate alignment is achieved before insertion so that jamming is not considered. Meanwhile, the spring is usually short and the contact force is limited within a small range, and as a result, other spring shapes, e.g., buckling, will not happen. According to this assumption, quadratic function is used to approximate the spring curve based on the distance of its two ends. For vertical insertion, the two cylinders are both vertical and the spring can be separated into two equal parts, which can be represented by quadratic functions.

Set the origin of the coordinates at the top spring end with the x-axis horizontally to the right and the z-axis vertically to the bottom, as shown in Fig. 1(b). Label $[x_e, z_e]^{\mathrm{T}}$ as the position of the spring's bottom end and $[F_x, F_z]^{\mathrm{T}}$ as the spring force. The spring curve is expressed as

$$x = \begin{cases} a_1 z^2 + b_1 z + c_1, & z < \dfrac{z_e}{2} \\ a_2 z^2 + b_2 z + c_2, & \text{otherwise} \end{cases} \tag{1}$$

where a, b, and c are the function parameters. The spring curve is differential and continuous with zero slopes at the two ends, according to which the function parameters result in

$$a_1 = -a_2 = \frac{2x_e}{z_e^2}, \quad b_1 = c_1 = 0, \quad b_2 = \frac{4x_e}{z_e}, \quad c_2 = -x_e. \tag{2}$$

The spring length yields

$$L = 2\int_0^{\frac{z_e}{2}} \sqrt{1 + 4a_1^2 z^2}\, dz \tag{3}$$

where L is the spring length. Label θ_l as the angle between the spring at l and z-axis, where l is the distance to the spring's top end, as shown in Fig. 1(b). The vertical force is acquired by integrating the projection of the curved spring onto the z-axis

$$F_z = \int_0^L k\frac{L_0 - L}{L}\cos\theta_l dl = k\left(\frac{L_0}{L} - 1\right) z_e \tag{4}$$

where L_0 is the spring length with no load. Correspondingly, the horizontal force can be obtained

$$F_x = k\left(\frac{L_0}{L} - 1\right) x_e. \tag{5}$$

If the spring force is known, usually measured from the force sensor, searching methods can be applied to acquire the offset between the spring's two ends, since the pairs $[x_e, z_e]^{\mathrm{T}}$ and $[F_x, F_z]^{\mathrm{T}}$ are one-to-one correspondence. To do that, resorting to (4) and (5), the following equation yields:

$$x_e = \frac{F_x}{F_z} z_e \tag{6}$$

which restricts the ratio between the vertical and horizontal offsets of the spring. Commonly, the vertical force is nonzero if the spring is stressed and (6) holds. With this ratio, the 1-D searching method can be used to find the spring length by minimizing the following function:

$$\begin{aligned} &\min \quad \left\| \frac{L_0 k z_e}{F_z + k z_e} - 2\int_0^{\frac{z_e}{2}} \sqrt{1 + 4a_1^2 z^2}\, dz \right\| \\ &\text{s.t. } x_e F_z - F_x z_e = 0 \end{aligned} \tag{7}$$

where the first part of the function to be minimized is the spring length computed from (4) and the second part is the spring length from (3). The spring state $[x_e, z_e]$ is obtained by optimizing the above function.

C. Compliance Analysis

The horizontal distance between the spring's two ends is x_e, which represents the offset between the gripper and the lower cylinder, and the horizontal force is F_x indicating the spring's force when the spring's ends are deviated. Therefore, the spring's horizontal stiffness results in

$$k_h = \frac{F_x}{x_e} = k\left(\frac{L_0}{L} - 1\right) \tag{8}$$

where k_h is the horizontal stiffness reflecting the ratio between the horizontal force and the offset. It shows that this horizontal stiffness increases monotonically with the decreasing spring length, with the lower bound being zero when the spring is not loaded. The spring's vertical stiffness yields

$$k_v = \frac{F_z}{L_0 - z_e} = \frac{k\,(L_0 - L)\,z_e}{L\,(L_0 - z_e)} \tag{9}$$

where k_v is the vertical stiffness of the spring. Combining the above two equations leads to $(k_h/k_v) = (z_e/L_0 - z_e)$, which means the larger the projection of the spring's length onto the z-axis, the smaller the horizontal stiffness than the vertical one. If the horizontal displacement x_e is very small, substituting $L = z_e$ into the above equation leads to $k_v = k$.

For a motionless lower cylinder in the hole, the spring force equals the contact force generated by the hole on the lower cylinder. In the scale of micrometers, we model the horizontal contact being linear to elastic deformation

$$F_x = M\Delta x_o \tag{10}$$

where Δx_o is the deformation between the lower cylinder and the hole, and M is the proportional factor between the material deformation and the exerted force. Besides, according to (8), when the spring's compression is small, which is very common in precision assembly, the spring's length is close to its free length, which yields that the horizontal stiffness k_h is much less than M. The resultant horizontal force on the lower cylinder is zero, which leads to

$$k_h x_e - M\Delta x_o = 0. \tag{11}$$

For a compressed spring, x_e and Δx_o locate on different sides of the hole's axis. To compensate for the lower object's misalignment, the upper gripper's movement depends on the magnitudes of spring displacement and object deformation

$$\Delta x_c = x_e - \Delta x_o \tag{12}$$

where Δx_c is the motion of the upper gripper in order to align the lower cylinder and the hole. Since k_h is smaller than M, the case that Δx_c is zero while F_h is nonzero does not occur, and $x_e > \Delta x_o$. Combining the above two equations leads to

$$k_c = \frac{F_h}{\Delta x_c} = \frac{Mk_h}{M - k_h} \tag{13}$$

where k_c is the assembly stiffness with a compressed spring. Comparing (10) and (13), the assembly compliance of a compressed spring is $M - k_h/k_h$ times rigid gripping. It means that the compressed spring has more compliance if $k_h < (M/2)$, and since k_h is much less than M, this configuration with spring has a considerable compliance in insertion.

III. Insertion Control

The insertion of a partially flexible object is a process where both rigid insertion and compliant insertion occur and it renders different control methods in different phases. We analyze the insertion process, propose control strategies for each stage, and present the efficient insertion planning.

A. Insertion Process Analysis

The whole insertion can be split into two processes: one cylinder is in the hole and both the cylinders are in contact with the hole. The insertion is initialized in the state where the spring is in its natural state and the object is aligned with the hole, as shown in Fig. 2(a).

Fig. 2(b) shows the first stage, where only the lower cylinder is inserted in the hole and the force sensor reflects the contact between this cylinder and the hole. It is a compliant insertion and the lower cylinder's state depends not only on the gripper's motion but also on the contact with the hole. This contact determines that the lower cylinder is not much deviated from the hole's center and the horizontal compensation is based on the horizontal force and compliance. Meanwhile, the uncalibrated insertion direction $\boldsymbol{d}$ should be estimated, and due to the insertion compliance, the method of estimating while inserting can be applied without exerting too much force on the cylinder.

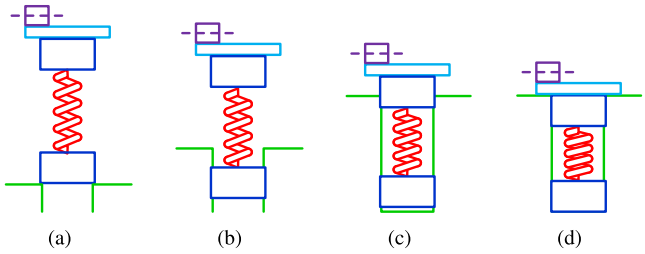

Fig. 2. Different states in the insertion process. (a) Initial configuration. (b) Compliant insertion. (c) Hybrid insertion. (d) Terminated configuration.

After the horizontal adjustment and direction estimation in the above stage, the upper gripper should be aligned with the hole's axis and this provides a good condition for the insertion of the upper cylinder. Fig. 2(c) shows the second insertion process, starting after the upper cylinder contacts with the hole. In this phase, the force sensor displays the resultant force that the hole exerts on both the cylinders, and thus the accurate individual states of each cylinder cannot be obtained. This insertion presents two different compliant types simultaneously: the insertion of the upper cylinder is a rigid one, since it is rigidly gripped by the upper gripper; and the insertion of the lower cylinder is a compliant one as it is connected to the upper cylinder through a spring. Therefore, it is a hybrid insertion. Both the cylinders' deviations from the hole's axis are not large and the control strategy is proposed after analysis on all possible configurations.

The whole insertion ends after the object is totally inserted, as shown in Fig. 2(d).

B. Compliant Insertion Process

The force sensor provides the force that the hole exerts on the lower cylinder. According to the current force $\boldsymbol{F}_t$, its decomposition results in

$$\boldsymbol{F}_{v,t} = (\boldsymbol{F}_t \cdot \boldsymbol{z})\boldsymbol{z}, \quad \boldsymbol{F}_{h,t} = \boldsymbol{z} \times \boldsymbol{F}_t \times \boldsymbol{z} \tag{14}$$

where $\boldsymbol{F}_{v,t}$ is the vertical force, $\boldsymbol{F}_{h,t}$ is the horizontal force, $\boldsymbol{z}$ is the vertical axis, "$\cdot$" is the dot product, and "$\times$" is the cross product.

The insertion controller consists of two parts: vertical insertion and horizontal compensation. The insertion depth increment is planned based on the previous performance, the current state, and the future insertion prediction, and an incremental PI controller is used for the horizontal compensation

$$\begin{cases} \Delta \boldsymbol{v}_{1,t+1} = \xi_{1,t}\Delta \boldsymbol{v}_{1,t} \\ \Delta \boldsymbol{h}_{1,t+1} = \dfrac{1}{k_{c,t}}[k_{p1}(\Delta \boldsymbol{F}_{h,t} - \Delta \boldsymbol{F}_{h,t-1}) + k_{i1}\Delta \boldsymbol{F}_{h,t}] \\ \qquad\qquad +\Delta \boldsymbol{v}_{1,t+1} \times \boldsymbol{d}_t \times \boldsymbol{z} \end{cases} \tag{15}$$

where $\Delta \boldsymbol{F}_{h,t}$ is the error between the desired and current horizontal forces, $\Delta \boldsymbol{v}_{1,t}$ is the current insertion vector of this first stage, $\Delta \boldsymbol{h}_{1,t}$ is the current compensation vector, $\xi_{1,t}$ is a parameter between two consecutive insertions, and k_{p1} and k_{i1} are

the proportional and integral parameters. The parameter $\xi_{1,t}$ is planned to efficiently fulfill insertion while considering the contact force. The last part of the second equation is the compensation for the horizontal projection of the inclined insertion based on the current estimated insertion direction $\boldsymbol{d}_t$.

For the unknown insertion direction $\boldsymbol{d}$, we present an approach to gradually estimate it and the strategy of estimating while inserting is used in order not to reduce the insertion efficiency. The spring state is determined according to the horizontal contact force, and then the deviation of the gripper relative to the hole's axis is computed. Replacing F_x and F_z in (6) and (7) with $\|\boldsymbol{F}_{h,t}\|_2$ and $\|\boldsymbol{F}_{v,t}\|_2$, the spring length is acquired using $x_{e,t}$ and $z_{e,t}$ to represent the distance between the spring's two ends at time t. Meanwhile, the lower cylinder's deviation from the hole's axis yields

$$\Delta \boldsymbol{x}_{l,t} = -\frac{\boldsymbol{F}_{h,t}}{M} \tag{16}$$

where $\Delta \boldsymbol{x}_{l,t}$ represents the distance vector from the hole's axis to the lower cylinder's center. The deviation of the upper cylinder relative to its alignment state results in

$$\Delta \boldsymbol{x}_{u,t} = x_{e,t}\frac{\boldsymbol{F}_{h,t}}{\|\boldsymbol{F}_{h,t}\|_2} + \Delta \boldsymbol{x}_{l,t} \tag{17}$$

where $\Delta \boldsymbol{x}_{u,t}$ is the distance vector from the hole's axis to the upper cylinder's center. The inclined insertion direction has consistent effects on the horizontal compensation

$$\Delta \overline{\boldsymbol{x}} = \Delta \boldsymbol{x}_{u,t} - \Delta \boldsymbol{x}_{u,t-n_1} + \sum_{i=0}^{n_1-1} [\|\boldsymbol{d}_t \cdot \boldsymbol{z}\| \Delta \boldsymbol{v}_{1,t-i} - \Delta \boldsymbol{h}_{1,t-i}] \tag{18}$$

where n_1 means how many steps to look back and $\Delta \overline{\boldsymbol{x}}$ is the insertion vector accumulated in n_1 steps. In the above equation, the third part on the right-hand side is the accumulated projection of the insertion onto the vertical axis, and the last part is the accumulated horizontal compensational motion. Due to disturbances, an approximation method is used to gradually estimate the direction

$$\overline{\boldsymbol{d}}_{t+1} = \gamma_1 \left(\frac{\Delta \overline{\boldsymbol{x}}}{\|\Delta \overline{\boldsymbol{x}}\|_2} - \boldsymbol{d}_t \right) + \boldsymbol{d}_t \tag{19}$$

where $\overline{\boldsymbol{d}}_{t+1}$ contains the direction of $\boldsymbol{d}_{t+1}$ and γ_1 discounts the estimation error. After unitization, the direction is estimated as

$$\boldsymbol{d}_{t+1} = \frac{\overline{\boldsymbol{d}}_{t+1}}{\|\overline{\boldsymbol{d}}_{t+1}\|_2}. \tag{20}$$

The estimation is terminated when the updating magnitudes are persistently small

$$\tilde{\boldsymbol{d}} = \boldsymbol{d}_t$$
$$\text{s.t. } \max\{\underbrace{\|\boldsymbol{d}_t - \boldsymbol{d}_{t-1}\|_2, \cdots, \|\boldsymbol{d}_{t-n_2+1} - \boldsymbol{d}_{t-n_2}\|_2}_{n_2}\} \leq \varepsilon \tag{21}$$

where ε is a positive parameter, n_2 is the persistent steps, and $\tilde{\boldsymbol{d}}$ is an approximation to the real direction. The checking of the last n_2 steps confirms whether the estimation is well done.

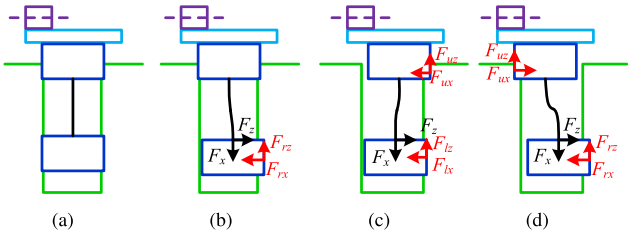

Fig. 3. (a)–(d) Configurations when the two cylinders contact with the hole, where F_{ux} and F_{uz} are the contact forces upon the upper cylinder from the hole and F_{lx} and F_{lz} are upon the lower cylinder.

C. Hybrid Insertion Process

The properties of this process include that: 1) the two contacting cylinders have different connecting types: rigid and compliant connecting in series; 2) the force sensor provides a resultant force the hole exerts; and therefore 3) the cylinders' states cannot be accurately determined. Facing these difficulties, we give an assumption that in the previous stage, the axis of the upper cylinder is adjusted to be close to the hole's axis and the insertion direction $\boldsymbol{d}$ is well estimated. This assumption is reasonable in that the insertion distance incorporating the lengths of the lower cylinder and the spring is basically long enough for adjustment and estimation.

Considering the physical constraints, there are four configurations to discuss, as shown in Fig. 3. Fig. 3(a) shows the expected state, in which the two cylinders are both well aligned with the zero horizontal force. Fig. 3(b) shows the configuration where only the upper cylinder is well aligned. In Fig. 3(c), the two cylinders are deviated in the same direction, with the lower cylinder less deviated, and Fig. 3(b) presents the two cylinders deviating in different sides.

Not all these configurations occur in insertion, and one is picked off qualitatively to simplify later discussion. This impossible configuration comes from the deviated cylinders in the same side. This setting only occurs when the spring is stretched, where the spring pulls the lower cylinder back in order to decrease the cylinder misalignment. Since during the insertion in the interference fit, the spring is compressed, and in this setting, the lower cylinder is definitely not still, since the spring and the hole generate horizontal forces in the same direction. Therefore, Fig. 3(c) is out of consideration. Below we quantitatively analyze the other two cases that are not aligned.

The configuration in Fig. 3(b) leads to $\Delta x_o = x_e$ and substituting it into (11) results in $k_h = M$. It means that this case only occurs in instantaneous states where the spring length is $L = (kL_0/M + k)$. This is a strict condition, and with the assumption of the upper cylinder having been aligned close to the hole's axis, the horizontal stiffness of the spring is much smaller than M. Therefore, the above equation cannot be satisfied, and then, this case is not possible in practice.

In Fig. 3(d), the resultant force on the lower cylinder yields

$$M\,(x_e - x_u) - k_h x_e = 0. \tag{22}$$

This equation requires $k_h < M$, which fits in the precision assembly. Rearranging (22) leads to $(x_e/x_u) = (M/M - k_h) \approx 1$, showing that the spring's horizontal spread

is only a little larger than the upper cylinder's misalignment. That means the lower cylinder is much closer to the hole's axis than the upper one.

After the above analysis, we conclude that Fig. 3(d) shows the only case to be considered if the force sensor outputs a nonzero horizontal value and the lower cylinder's misalignment is quite small. Therefore, we can use the controller for rigid gripping to deal with the hybrid insertion, ignoring the horizontal force on the lower object. This controller also includes vertical insertion and horizontal compensation

$$\begin{cases} \Delta \boldsymbol{v}_{2,t+1} = \xi_{2,t} \Delta \boldsymbol{v}_{2,t} \\ \Delta \boldsymbol{h}_{2,t+1} = \dfrac{1}{M}[k_{p2}(\Delta \boldsymbol{F}_{h,t} - \Delta \boldsymbol{F}_{h,t-1}) + k_{i2} \Delta \boldsymbol{F}_{h,t}] \\ \qquad\qquad + \Delta \boldsymbol{v}_{2,t+1} \times \tilde{\boldsymbol{d}} \times \boldsymbol{z} \end{cases} \tag{23}$$

where $\Delta \boldsymbol{v}_{2,t}$ and $\Delta \boldsymbol{h}_{2,t}$ are the vectors of vertical insertion and horizontal compensation in the second stage, k_{p2} and k_{i2} are another proportional and integral parameters, $\tilde{\boldsymbol{d}}$ is the insertion direction estimated in the previous stage, and $\xi_{2,t}$ is the insertion parameter. The horizontal compensation difference between the controllers of the two stages lies in the horizontal compliance: one is with a spring and the other is rigid.

D. Insertion Planning

The compliant mechanism brings uncertainty, and for efficiency improvement, the insertion is planned based on the past performance, the current contact evaluation, and the future insertion prediction.

1) First Stage: In the first insertion stage, a large misalignment of the upper gripper only results in a small deviation of the lower object. Therefore, aggressive methods can be taken to improve the efficiency.

Due to the connecting spring, the two cylinders' insertion depth increments are not naturally equal, and this difference is reflected by

$$\sigma_{v,t} = \frac{\|\Delta \boldsymbol{z}_{l,t}\|_2}{\|\Delta \boldsymbol{z}_{u,t}\|_2} = 1 + \frac{z_{e,t} - z_{e,t-1}}{\Delta \boldsymbol{v}_{1,t} \cdot \boldsymbol{d}_t} \tag{24}$$

where $\Delta \boldsymbol{z}_{l,t}$ and $\Delta \boldsymbol{z}_{u,t}$ are the vertical insertion depth increments of the lower and upper cylinders, and $\sigma_{v,t}$ is the insertion ratio between the insertions of the two cylinders. $\sigma_{v,t} < 1$ means the spring is more compressed; $\sigma_{v,t} = 1$ represents that the cylinders' insertion depth increments are equal; and otherwise, the lower cylinder inserts more. We can use the previous insertion ratios to estimate the next ratio

$$\overline{\sigma}_{v,t+1} = \gamma_2 \sigma_{v,t} + (1 - \gamma_2) \frac{\sum_{j=0}^{n_3-1} \gamma_3^j \sigma_{v,t-j}}{\sum_{j=0}^{n_3-1} \gamma_3^j} \tag{25}$$

where $\overline{\sigma}_{v,t+1}$ is the estimated ratio for the next step, γ_2 and γ_3 are the discounted parameters, and n_3 means how many previous ratios are used. The next ratio is estimated with the discounted sum of the current ratio and multiple previous ones.

The contact state for the first stage incorporates the horizontal force and the insertion direction estimation error. We can use an aggressive factor to evaluate the horizontal force, since most of the misalignment can be counteracted by the spring

$$\alpha_t = \max\left\{1 - \frac{\|\boldsymbol{F}_{h,t}\|_2 - T_{n1}}{T_{n1}}, 1 - \frac{\|\boldsymbol{F}_{h,t}\|_2 - \|\boldsymbol{F}_{h,t-1}\|_2}{k_f}\right\} \tag{26}$$

where α_t is the evaluation factor relating to the horizontal force, and T_{n1} and k_f are constant parameters. The first part in the bracket values larger than 1 if the horizontal force is less than T_{n1}, and the second part gives a value larger than 1 if the horizontal force is decreasing. The maximum function means that only when the horizontal force surpasses T_{n1} and grows large, the evaluation factor is less than one, which means that the current contact state needs to slow the insertion. The expected insertion depth increment of the next step yields

$$\Delta \overline{v}_{1,t+1} = \frac{\alpha_t (1 - k_d \|\boldsymbol{d}_t - \boldsymbol{d}_{t-1}\|_2) \|\Delta \boldsymbol{x}_{l,t}\|_2}{\overline{\sigma}_{v,t+1}} \tag{27}$$

where $\Delta \overline{v}_{1,t+1}$ is the expected insertion depth increment of the next step and k_d is a scaling parameter. In (27), the part in the bracket evaluates the estimation of the insertion direction; the numerator computes the lower cylinder's expected insertion depth increment based on the two factors reflecting the current contact state and the current insertion depth increment; and dividing this expected insertion depth increment by the expected insertion ratio results in the upper gripper's expected insertion depth increment. The insertion parameter is obtained by limiting the above result

$$\xi_{1,t} = \frac{\min\{\Delta \overline{v}_{1,t+1}, \Delta v_{1,\max}\}}{\|\Delta \boldsymbol{v}_{1,t}\|_2} \tag{28}$$

where $\Delta v_{1,\max}$ is the maximum insertion depth increment in the first stage.

The switch condition to the next stage can be set as the total insertion distance of the lower cylinder and the spring

$$\mathscr{L}_t - \mathscr{L}_1 > 0 \tag{29}$$

where $\mathscr{L}_t = \sum_{i=1}^{t} \Delta \boldsymbol{v}_{1,i} \cdot \boldsymbol{z}$ is the inserted distance and $\mathscr{L}_1$ is the desired insertion distance for the first stage. When $\mathscr{L}_t$ is close to $\mathscr{L}_1$, the last step inserts the upper object to be in the initial state of the next stage.

2) Second Stage: In this hybrid insertion, the states of cylinders are not accurately obtained and the compliance only applies to one cylinder with the other one rigidly gripped. Therefore, the insertion planning is conservative and different from the above method.

Define an internal parameter based on the horizontal contact and the insertion depth increment

$$\beta_{t+1} = \min\left\{2e^{-\frac{\gamma_4 \|\boldsymbol{F}_{t,h}\|_2}{\|\Delta \boldsymbol{v}_{2,t}\|_2}} \beta_t,\ \beta_{\max}\right\} \tag{30}$$

where γ_4 is a scaling parameter and β_t is an updating internal parameter, which is limited by its maximum allowed value $\beta_{\max}$. This internal parameter concerns about both safety and efficiency: a big parameter corresponds to a small horizontal force with a large insertion depth increment. The ratio between two consecutive internal parameters ranges in (0, 1]. The parameter β_t can be seen as a result of historical states, updated in each time step rather than just based on

the current performance. The initial value of this parameter correlates with the insertion ratio of the previous stage. Let t_s be the time step when the stage switches and the initial value yields

$$\beta_{t_s} = \frac{\xi_{1,t_s-2}\|\Delta \boldsymbol{v}_{1,t_s-2}\|_2 \beta_{\max}}{\Delta v_{1,\max}} \tag{31}$$

where β_{t_s} is the initial magnitude of β_t. It is computed according to the ratio of the next to last time step before the stage switch. The reason not to use the time step $t_s - 1$ is because this last step initializes for the second stage, and not the representation of the insertion efficiency of the first stage.

The insertion parameter for this stage is planned

$$\xi_{2,t} = \min\left\{[1 + (\beta_t - T_{n2})]\left[1 - \frac{\gamma_5\left(\|\boldsymbol{F}_{v,t}\|_2 - T_{n3}\right)}{T_{n3}}\right], \frac{\Delta v_{2,\max}}{\|\Delta \boldsymbol{v}_{2,t}\|_2}\right\} \tag{32}$$

where T_{n2} is a parameter above which the parameter β_t has a positive effect on increasing the insertion depth increment, T_{n3} is a parameter related to the vertical force, $\Delta v_{2,\max}$ is the maximum insertion depth increment allowed in the second stage, and

$$\gamma_5 = \begin{cases} 1, & \|\boldsymbol{F}_{v,t}\|_2 - T_{n3} > 0 \\ 0. & \text{otherwise.} \end{cases} \tag{33}$$

It means that only when the internal parameter β_t is larger than T_{n2} and the vertical force is within T_{n3}, the insertion depth does start to grow. Generally, the maximum insertion depth increment of the second stage is less than the first stage, $\Delta v_{2,\max} < \Delta v_{1,\max}$.

The end condition of the insertion is set as the union of the inserted distance and the vertical force

$$\mathscr{L}_t - \mathscr{L}_2 > 0 \cup F_{v,m} - \|\boldsymbol{F}_{v,t}\|_2 < 0 \tag{34}$$

where $\mathscr{L}_2$ is the desired insertion distance for the whole insertion and $F_{v,m}$ is the maximum allowed vertical force. If the hole's depth is shorter than the sum of two cylinders' lengths and the spring's free length, the lower cylinder touches the bottom of the hole and the spring starts to be more compressed, right before the upper cylinder reaches its terminal position. The spring's vertical force is expected to be accumulated, and if the horizontal force is not large, a fix insertion depth increment is used to insert the object to its terminal state.

Fig. 4 shows the insertion control process for the partially flexible object. For the first stage, according to the measured force, the spring state is obtained and the assembly stiffness is computed. With the spring state, the insertion ratio is calculated, and furthermore, the next ratio is estimated. Based on the current spring state, the insertion direction is estimated via computation of misalignment and the estimation error effect. The expected insertion depth increment is then planned and limited by its maximum allowed threshold and the horizontal compensation is acquired based on the horizontal force, the estimated direction, and the assembly stiffness. For the second stage, the internal parameter β_t is updated, given the current horizontal force and the previous insertion

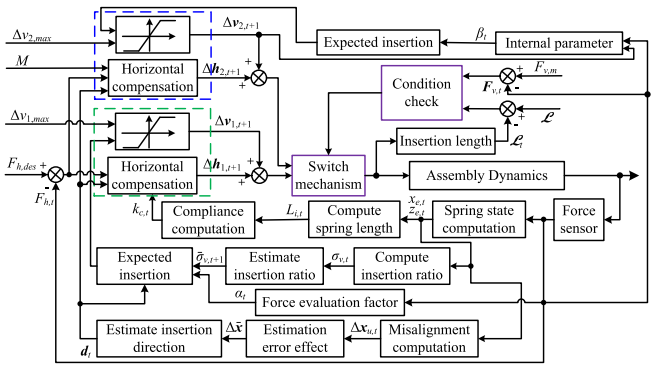

Fig. 4. Insertion control process for a partially flexible object.

depth increment. The insertion depth increment is accordingly planned and limited and the compensation in the horizontal plane is computed on the basis of the horizontal force and the estimated direction. The switch mechanism determines which controller works and the output is sent to the actuators. The condition check function activates the switch based on checking results of the vertical force and the inserted distance.

The insertion in this paper is a discrete control process and the manipulators are driven with stepper motors, which can be modeled to a one-order inertial element and an integral element. The control system is stable with well-tuned parameters of the PI controller. In the first insertion phase, the axis of the upper cylinder is adjusted to be close to the axis of the hole, and the phase switch will not cause big changes or oscillation in the radial contact force. With appropriate controller parameters, the switch between the two phases does not affect the system stability.

IV. Experiments

The insertion strategies are testified on a precision assembly platform, which is shown in Fig. 5. It equips with three microscopes, two force sensors, and six robot arms, but for this experiment, only two arms, two microscopes, and a force sensor are used to verify the insertion strategy. The upper arm holds the upper cylinder and is equipped with three linear ball guides, Suguar KWG06030-G whose translational resolution is ± 0.5 μm, to achieve 3-D translational movement, and a two-axis rotation stage, Sigma KKD-25C, for two-DOF manual tilt adjustment. The lower arm, which grips the hole, has an elevator stage, Micos ES-100, with movement errors within 0.1 μm to fulfill the insertion and three motorized goniometer stages, KGW06050-L, KGW06075-L, and SGSP-40yaw for rotation. The horizontal microscopes are GC2450 with a resolution of 2448×2050 pixels and PointGrey 50S5M-C whose resolution is 2448×2048 pixels, and the force sensor is Nano-43 with a resolution of 1/128N, which can be improved with filtering. Both the cylinders are hollow with 0.1-mm thickness, 3-mm length, and 3-mm diameter. The object containing the hole is a hollow cylinder with 50-μm thickness and 9.4-mm length. The materials are aluminum. The hole has the same diameter as the cylinders with the magnitude of interference between them lying in $0\sim5$ μm. The compression spring is 3.5-mm long and its diameter is 1.2 mm.

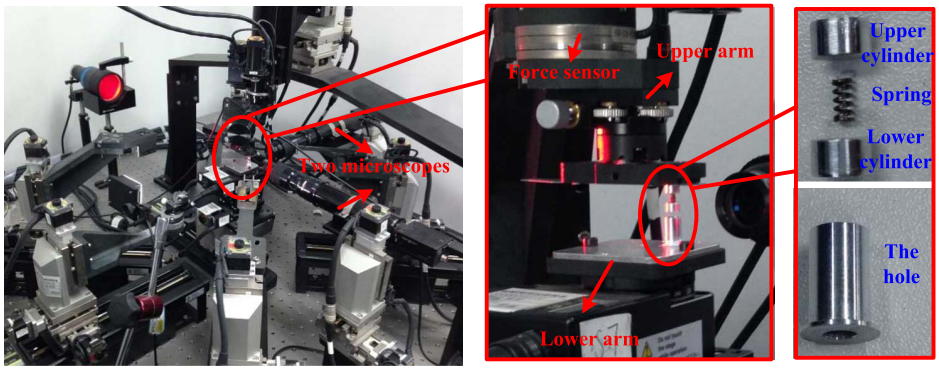

Fig. 5. Assembly platform and the object.

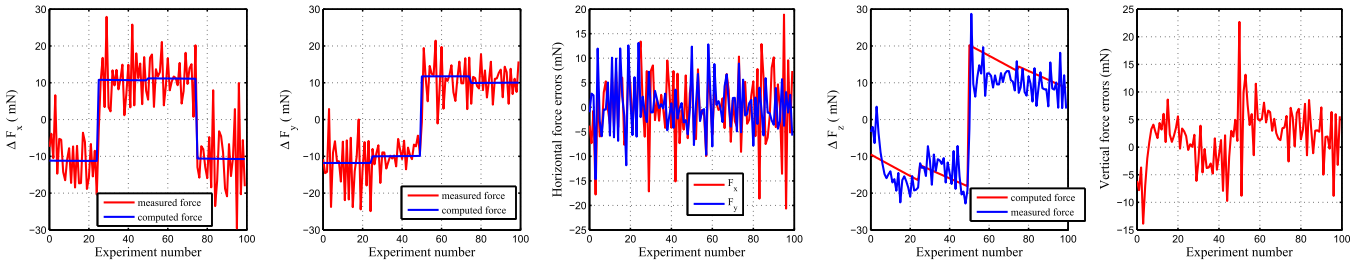

Fig. 6. Comparison between the forces computed from the spring model and measured from the force sensor. (a), (b), and (d) Relative forces in the x-, y-, and z-axes between two consecutive states. (c) and (e) Horizontal and vertical errors between the computed force and the measured force.

TABLE I
PARAMETERS FOR EXPERIMENTS

M	$\Delta v_{1,max}$	k_{p1}, k_{p2}	γ_1	γ_3	k_d	T_{n1}	$n_1 \sim n_3$
67mN/μm	10 μm	0.3	0.2	0.8	0.2	100	0.5
k	$\Delta v_{2,max}$	k_{i1}, k_{i2}	γ_4	γ_2, γ_5	k_f	T_{n2}	T_{n3}
27.4mN/μm	5μm	0.5	0.005$ln2$	0.5	100mN	0.5	500

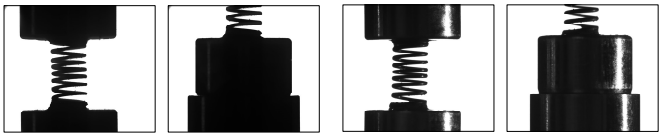

Fig. 7. Insertion initialization. (a) and (b) Views in the microscopes 1 and 2. In each subfigure, the left shows the object and the right shows the alignment between the object and the hole.

Using the least square method, we calibrate the rotational matrix from the force sensor to the upper robot arm. The spring coefficient is obtained averaging the ratios between the force and the compressed length from several experiments. The proportional factor M is calibrated by averaging the ratios between the horizontal movements and the horizontal force changes when the rigidly gripped object contacts the hole. The maximum insertion step for the first stage is twice that of the second stage, showing a restricted limitation for hybrid insertion. The parameters are shown in Table I. The upper manipulator is a little deviated from the vertical, which is set as the initial guess of this insertion direction. We use the Ziegler–Nichols method to regulate the controller parameters and the Butterworth method to filter the force sensor.

We first experiment to verify the spring model by comparing the computed and measured forces. The upper gripper moves 25 steps of 2 μm sequentially along the positive x-axis, the positive y-axis, the negative x-axis, and the negative y-axis in its own coordinates. The force change between two steps is picked as the comparison objective. Using these movements and the corresponding forces, we can optimize the initial offset and compute the force changes corresponding to the movements. The comparison results are shown in Fig. 6, where Fig. 6(a)–(c) shows the relative horizontal forces and the errors and Fig. 6(d) and (e) shows the vertical forces and errors. The mean error is $\mu = [-0.01, 0.23, 1.83]^{\mathrm{T}}$ mN and the standard deviation is $\sigma = [7.28, 5.47, 5.27]^{\mathrm{T}}$ mN. All these show that the proposed spring model presents a relationship between the force and its offset with a tolerant approximation error.

The proposed method is used to insert the object into the hole. The insertion initialization is shown in Fig. 7, where the object state and the alignment between the object and the hole are presented. Fig. 8 shows the insertion performance, where the green dotted lines represent the switch between the two stages. In the first stage, the horizontal force is small, mostly less than 50 mN and the vertical force is within 100 mN, and therefore, the insertion in this stage is at its maximum insertion step. The horizontal compensation motion is shown in Fig. 8(a), and since the minimum movement of the actuators is 1 μm, this compensational curve is zigzag-like. The maximum horizontal displacement is about 125 μm in the x-direction and 50 μm in the y-direction, which decreases the horizontal force. The average stiffness in this stage is 8.9 mN/μm, and comparing with rigid clamping, its compliance is about eight times. Fig. 8(c) shows the lower cylinder's horizontal movement, calculated from the horizontal force,

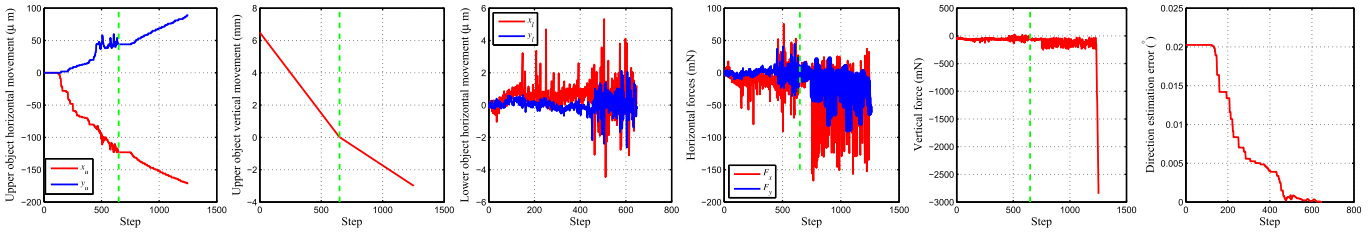

Fig. 8. Experimental results. (a) Upper cylinder's horizontal movements. (b) Upper cylinder's vertical movements. (c) Lower cylinder's horizontal movements, computed from the horizontal force. (d) Horizontal forces. (e) Vertical force. (f) Direction estimation error.

TABLE II
COMPARATIVE RESULTS

Our method				The method in [7]			
No.	Times(s)	No.	Times(s)	No.	Times(s)	No.	Times(s)
1	130	2	130	1	155.8	2	156.4
3	130.3	4	130.2	3	158.6	4	158.3

and it can be seen that this horizontal adjustment is very small. Fig. 8(f) presents the insertion direction estimation. Due to the restriction of the actuators' minimum movement, we change the estimation to a process that only when the horizontal compensation occurs, the estimation starts. The estimation error gradually approaches to zero, with a very small magnitude when this stage ends. The forces in the second stage is comparatively large, as shown in Fig. 8(d) and (e). It can be seen that the horizontal compensation movements in these two stages are almost the same, but the horizontal forces are quite different. This shows the compliance of the two stages from another aspect. Since the lower cylinder's state is not observable in the second stage, its state computation is not shown. Before the end of this insertion, the spring is more compressed and the vertical force increases to about 3N, as the hole's depth is 100 μm less than the insertion distance. In these last insertions, the maximum step is used since the horizontal force is still small. These experimental results show that the insertion direction can be well estimated and the proposed method is applicable to assemble partially flexible objects.

We also carry out comparative experiments with the method proposed in [7], which adjusts the insertion depth increments according to the contact force. In the comparative experiments, the maximum insertion depth increments are the same as the above and the parameters are the same as used in [7]. The objects are well aligned and no inclination is involved. We apply the insertion estimation approach in this comparative method and employ our spring model to compute the horizontal stiffness of the compliant insertion. The time interval is set to 0.1 s. We conduct four experiments on different objects and springs, which means different magnitudes of interference, different cylinders' diameters, and different uncertainties. Owing to the fact that the comparative controller also uses the same estimation and compliance, the forces between objects are similar, and as a result, their insertion efficiency is chosen as the comparison index. Table II shows the time cost used in each experiment where a deliberate disturbance of displacing the gripper during insertion is added in the last two experiments. Our method always takes the maximum insertion depth increment and spends 130 s; while the comparative method varies a little due to the different horizontal forces and uses about 157 s. Besides, we have conducted 30 experiments altogether and all insertions are successfully achieved. This shows the efficiency and repeatability of the proposed approach.

V. CONCLUSION

This paper considers the efficient insertion of the partially flexible object in precision assembly and solves the problems in hybrid insertion. A spring is picked as the example of the compliant connection due to its flexibility of compression, transverse, and bending. We first build a spring model to relate its state and the exerting force and then analyze the assembly stiffness. The first stage is a process of a compliant insertion and a control strategy is proposed to online-estimate the insertion direction, compensate for the horizontal misalignment, and plan an aggressive insertion based on the past performance, the current contact, and the insertion prediction. The second stage is a process of a hybrid insertion where the rigid and compliant clamping is in series. To solve the problem of immeasurable accurate state and the uncontrollable compliant part, we qualitatively and quantitatively analyze all the possible configurations, based on the built spring model, to distinguish the correct relative posture between the two rigid parts. A control strategy is also presented for horizontal compensation and conservative vertical insertion according to the effect of previous performance and the current evaluation. Several experiments are implemented to validate the proposed method.

REFERENCES

[1] H. Van Brussel *et al.*, "Assembly of microsystems," *CIRP Ann.*, vol. 49, no. 2, pp. 451–472, 2000.
[2] Y. Shen, W. Wan, H. Lu, T. Fukuda, and W. Shang, "Automatic sample alignment under microscopy for 360° imaging based on the nanorobotic manipulation system," *IEEE Trans. Robot.*, vol. 33, no. 1, pp. 220–226, Feb. 2017.
[3] B. Tamadazte, N. L.-F. Piat, and S. Dembélé, "Robotic micromanipulation and microassembly using monoview and multiscale visual servoing," *IEEE/ASME Trans. Mechatronics*, vol. 16, no. 2, pp. 277–287, Apr. 2011.
[4] R. C. Montesanti *et al.*, "Lessons from building laser-driven fusion ignition targets with the precision robotic assembly machine," *Fusion Sci. Technol.*, vol. 59, no. 1, pp. 70–77, 2011.
[5] D. Xing, D. Xu, F. Liu, H. Li, and Z. Zhang, "Precision assembly among multiple thin objects with various fit types," *IEEE/ASME Trans. Mechatronics*, vol. 21, no. 1, pp. 364–378, Feb. 2016.

[6] A. N. Das, R. Murthy, D. O. Popa, and H. E. Stephanou, "A multiscale assembly and packaging system for manufacturing of complex micro-nano devices," *IEEE Trans. Autom. Sci. Eng.*, vol. 9, no. 1, pp. 160–170, Jan. 2012.
[7] D. Xing, F. Liu, F. Qin, and D. Xu, "Coordinated insertion control for inclined precision assembly," *IEEE Trans. Ind. Electron.*, vol. 63, no. 5, pp. 2990–2999, May 2016.
[8] S. Liu, Y.-F. Li, D.-P. Xing, D. Xu, and H. Su, "An efficient insertion control method for precision assembly of cylindrical components," *IEEE Trans. Ind. Electron.*, vol. 64, no. 12, pp. 9355–9365, Dec. 2017.
[9] S. Liu, D. Xu, D. Zhang, and Z. Zhang, "High precision automatic assembly based on microscopic vision and force information," *IEEE Trans. Autom. Sci. Eng.*, vol. 13, no. 1, pp. 382–393, Jan. 2016.
[10] P. Jiménez, "Survey on model-based manipulation planning of deformable objects," *Robot. Comput.-Integr. Manuf.*, vol. 28, no. 2, pp. 154–163, 2012.
[11] M. Karlsson and S. Gong, "Circular dipole antenna for mode 1 UWB radio with integrated balun utilizing a flex-rigid structure," *IEEE Trans. Antennas Propag.*, vol. 57, no. 10, pp. 2967–2971, Oct. 2009.
[12] A. Izadbakhsh, "Robust control design for rigid-link flexible-joint electrically driven robot subjected to constraint: Theory and experimental verification," *Nonlinear Dyn.*, vol. 85, no. 2, pp. 751–765, 2016.
[13] B. Mimoun, V. Henneken, A. van der Horst, and R. Dekker, "Flex-to-rigid (F2R): A generic platform for the fabrication and assembly of flexible sensors for minimally invasive instruments," *IEEE Sensors J.*, vol. 13, no. 10, pp. 3873–3882, Oct. 2013.
[14] Z. Wang *et al.*, "Design of a novel compliant safe robot joint with multiple working states," *IEEE/ASME Trans. Mechatronics*, vol. 21, no. 2, pp. 1193–1198, Apr. 2016.
[15] N. Cai and L. Qiao, "Rigid-compliant hybrid variation modeling of sheet metal assembly with 3D generic free surface," *J. Manuf. Syst.*, vol. 41, pp. 45–64, Oct. 2016.
[16] H. Park, J. Park, D.-H. Lee, J.-H. Park, M.-H. Baeg, and J.-H. Bae, "Compliance-based robotic peg-in-hole assembly strategy without force feedback," *IEEE Trans. Ind. Electron.*, vol. 64, no. 8, pp. 6299–6309, Aug. 2017.
[17] S. Huang and J. M. Schimmels, "Admittance selection conditions for frictionless force-guided assembly of polyhedral parts in two single-point principal contacts," *IEEE Trans. Robot.*, vol. 24, no. 2, pp. 461–468, Apr. 2008.
[18] S.-K. Yun, "Compliant manipulation for peg-in-hole: Is passive compliance a key to learn contact motion?" in *Proc. IEEE Int. Conf. Robot. Automat.*, May 2008, pp. 1647–1652.
[19] Y. Li and Q. Xu, "A novel design and analysis of a 2-DOF compliant parallel micromanipulator for nanomanipulation," *IEEE Trans. Autom. Sci. Eng.*, vol. 3, no. 3, pp. 247–254, Jul. 2006.
[20] Q. Xu, "Robust impedance control of a compliant microgripper for high-speed position/force regulation," *IEEE Trans. Ind. Electron.*, vol. 62, no. 2, pp. 1201–1209, Feb. 2015.
[21] Y.-B. Bang, K.-M. Lee, J. Kook, W. Lee, and I.-S. Kim, "Micro parts assembly system with micro gripper and RCC unit," *IEEE Trans. Robot.*, vol. 21, no. 3, pp. 465–470, Jun. 2005.

Dengpeng Xing received the B.S. degree in mechanical electronics and the M.S. degree in mechanical manufacturing and automation from Tianjin University, Tianjin, China, in 2002 and 2006, respectively, and the Ph.D. degree in control science and engineering from Shanghai Jiao Tong University, Shanghai, China, in 2010.

He is currently an Associate Professor with the Research Center of Precision Sensing and Control, Institute of Automation, Chinese Academy of Sciences, Beijing, China. His research interests include robot control and learning, precision assembly, and optimization.

Fangfang Liu received the B.S. and Ph.D. degrees in mechanical electronics from Zhejiang University, Hangzhou, China, in 2006 and 2012, respectively.

She is currently an Associate Professor with the Research Center of Precision Sensing and Control, Institute of Automation, Chinese Academy of Sciences, Beijing, China. Her research interests include precision mechanical design and mechatronic control.

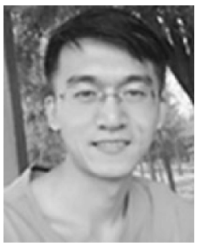

Song Liu received the B.Sc. degree in sensing technology and instrumentation from Shandong University, Jinan, China, in 2012, the Ph.D. degree in control science and engineering from the Institute of Automation, Chinese Academy of Sciences, Beijing China, and the Ph.D. degree from the Department of Mechanical and Biomedical Engineering, City University of Hong Kong, Hong Kong, in 2017.

He is currently a Post-Doctoral Fellow with the Robot Vision Research Laboratory, City University of Hong Kong. His research interests include visual measurement, visual servo control, microassembly, and micromanipulation.

De Xu (M'05–SM'09) received the B.S. and M.S. degrees from the Shandong University of Technology, Jinan, China, in 1985 and 1990, respectively, and the Ph.D. degree from Zhejiang University, Hangzhou, China, in 2001, all in control science and engineering.

Since 2001, he has been with the Institute of Automation, Chinese Academy of Sciences, Beijing, China, where he is currently a Professor with the Research Center of Precision Sensing and Control. His research interests involve robotics and automation, in particular the control of robots, such as visual control and intelligent control.